Electronic Supplementary Information

Silk Fibroin Films with Embedded Magnetic Nanoparticles: Evaluation of the Magneto-Mechanical Stimulation Effect on Osteogenic Differentiation of Stem Cells

Lucia Del Bianco[1&*], Federico Spizzo[1&], Yuejiao Yang[2&], Gabriele Greco[3], Maria Laura Gatto[4], Gianni Barucca[4], Nicola M. Pugno[3,5], Antonella Motta[2*]

[1] Department of Physics and Earth Science, University of Ferrara, I-44122 Ferrara, Italy

[2] BIOtech Research Center, Department of Industrial Engineering, University of Trento, I- 38123 Trento, Italy

[3] Laboratory for Bioinspired, Bionic, Nano, Meta, Materials & Mechanics, Department of Civil, Environmental and Mechanical Engineering, University of Trento, I-38123 Trento, Italy

[4] Department SIMAU, Università Politecnica delle Marche, I-60131 Ancona, Italy

[5] School of Engineering and Materials Science, Queen Mary University of London, Mile End Road, London E1 4NS, UK

[&] These authors contributed equally

[*]Corresponding authors:

L. Del Bianco (lucia.delbianco@unife.it), A. Motta (antonella.motta@unitn.it)

Transmission Electron Microscopy (TEM)

Transmission Electron Microscopy (TEM) analysis is performed by a Philips CM200 microscope (Philips, Amsterdam, The Netherlands) operating at 200 kV and equipped with a LaB6 filament.

Iron oxide NPs purchased from Iolitec GmbH (Germany) are subjected to routine analyses by TEM observations and selected area electron diffraction (SAED) measurements. To this end, a small quantity of NPs is dispersed in ethanol and subjected to ultrasonic agitation for approximately one minute. A drop of the suspension is deposited on a commercial TEM grid covered with a thin carbon film; finally, the grid is kept in air until complete evaporation of the ethanol.
As shown in Fig. S1a, the NPs tend to agglomerate on the TEM grid and high-resolution images reveal that most of them have a size of ~ 10 nm (Fig. S1b). The SAED pattern of the NPs is consistent with the spinel structure of magnetite, but traces of maghemite and hematite are also detected (Fig. S1c).

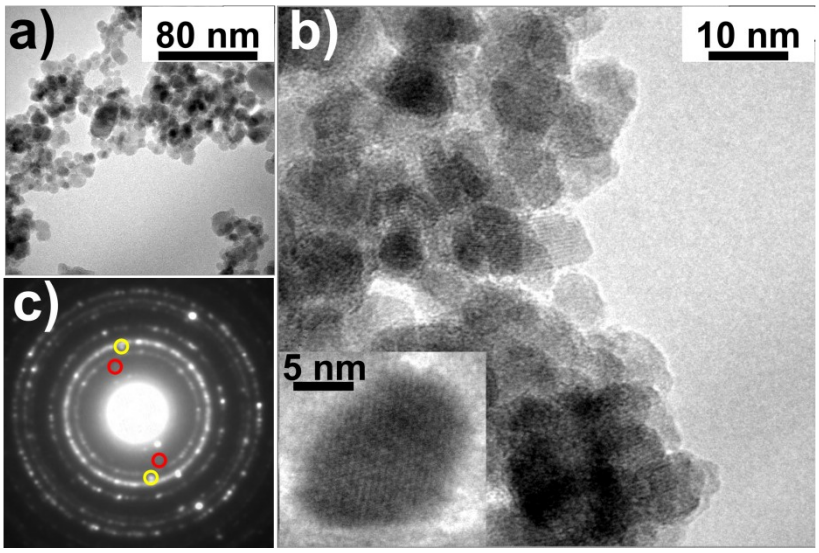

Fig. S1. a) bright field image of the magnetic NPs; b) high-resolution TEM image revealing that NPs are well crystalized (see inset) and have a typical dimension of ~ 10 nm ; c) typical selected area electron diffraction pattern: all the diffraction rings can be attributed to the magnetite phase, while few sporadic diffraction spots can be associated to the maghemite (red circles) or hematite (yellow circles) phases.

Portions of the HC film are embedded in epoxy resin (Sigma) and ultrathin cross sections 100-nm thick are obtained using an ultra-microtome (Sorvall MT 5000).
In the bright field image shown in Fig. S2a the magnetic NPs appear as dark agglomerates embedded in the fibroin matrix, which gives a light gray contrast. The nature of the NPs and their distribution in the fibroin matrix is investigated by SAED measurements and dark-field observations. In particular, the SAED pattern corresponding to the agglomerate of Fig. S2a is shown in the inset and all the diffraction spots can be attributed to the magnetite phase. Fig. S2b shows the corresponding dark-field image obtained with the diffraction spots evidenced by a circle in the SAED pattern. The regions of the sample responsible for the encircled diffraction spots appear bright and suggest that the large agglomerates are not compact ensembles of NPs, but are made up of smaller NP aggregates intimately mixed with the fibroin component. This description is confirmed by the High-resolution TEM image in Fig. S2C.

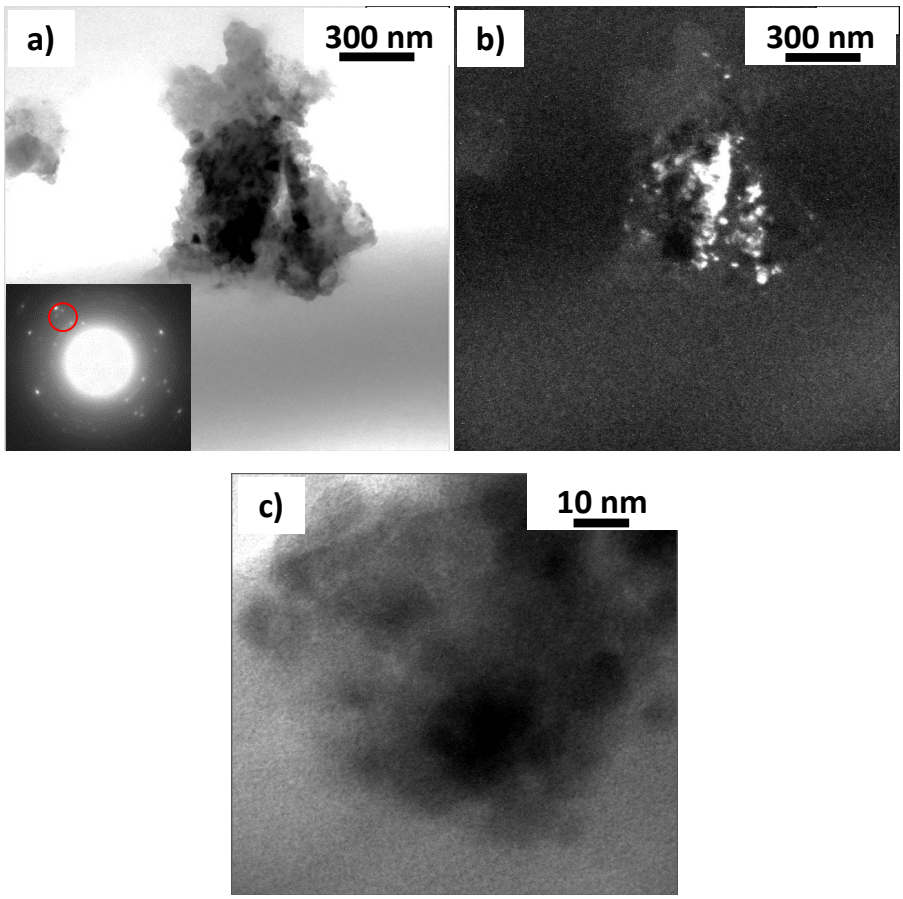

Fig. S2. a) TEM bright field image of a NP aggregate embedded in the fibroin matrix in the HC film and corresponding SAED pattern (inset); b) TEM dark field image of the same NP aggregate shown in a), obtained with the diffraction spot encircled in the SAED pattern. c) High-resolution TEM image of a NP aggregate in intimate contact with the silk fibroin matrix.

Hardness measured by nanoindentation

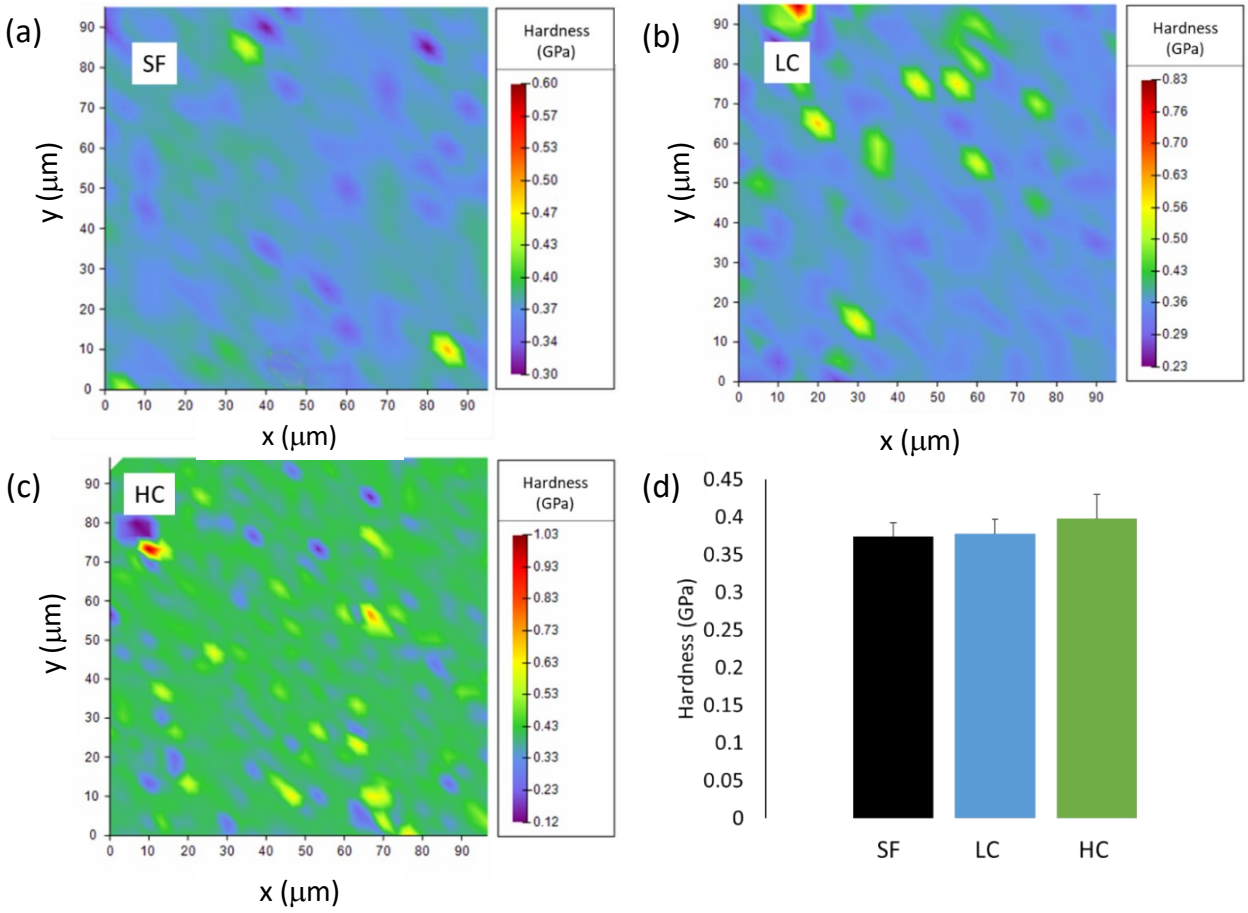

Fig. S3. Hardness distribution maps obtained by nanoindentation of films (a) SF, (b) LC and (c) HC. (d) Average values of the hardness for the three films.

Fourier transform infrared spectroscopic with attenuated total reflectance (FTIR-ATR)

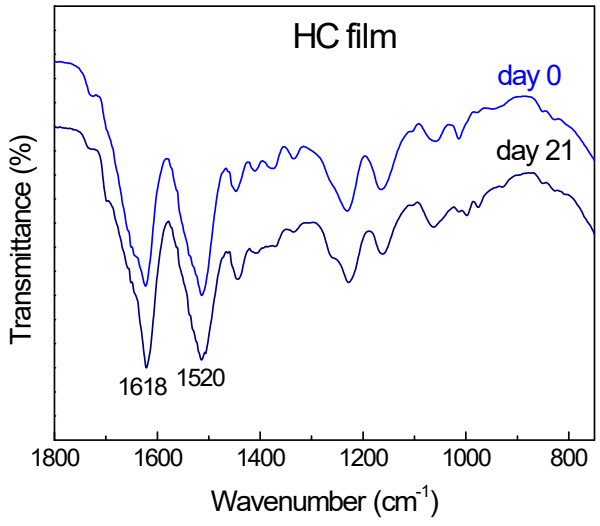

Fig. S4. FTIR_ATR spectra of film HC as-cast and after 21 days of incubation in the cell culture medium at 37°C.

Magnetic measurements by SQUID

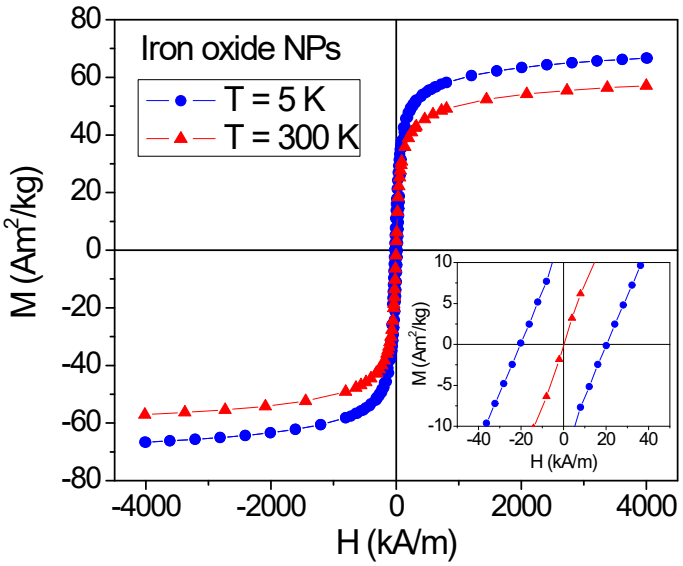

Fig. S5. Magnetic hysteresis loop measured on the iron oxide NPs in the form of powder, at T = 5 K and 300 K. The inset is an enlarged view of the central region of the loops.

The saturation magnetization of the iron oxide magnetic NPs, as measured by SQUID in an applied field H = 4×10^3 kA/m, is M_S = (66.7 ± 0.7) Am^2/kg at T = 5 K, a value well below that of bulk magnetite and maghemite (98 Am^2/kg and 83 Am^2/kg, respectively). The reduction of M_S is often observed in iron oxide NPs and attributed to spin canting and magnetic disorder effects and also to the coexistence of different oxide phases [Ref. 14; M. Coduri et al., *Nanomaterials* **2020**, *10* (5), 867], as indeed detected by SAED measurements (Fig. S1c). At T = 300 K, M_S = (57.1 ± 0.6) Am^2/kg and the coercivity is null, which is in favor of a superparamagnetic relaxing behavior of the NP magnetic moments.

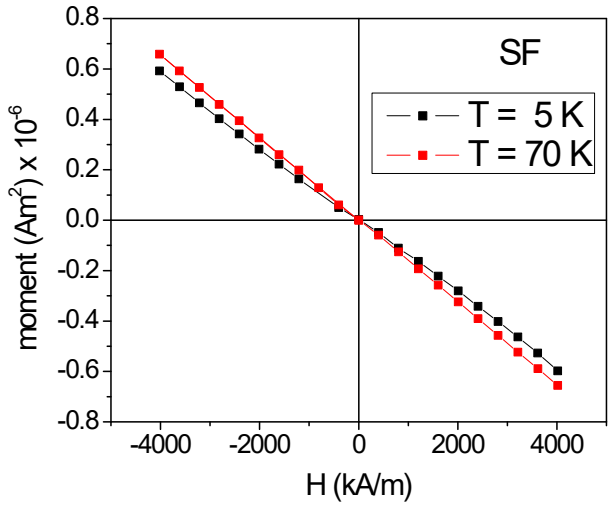

Fig. S6. Magnetic moment vs. magnetic field measured by SQUID on the dried silk fibroin film SF, at T = 5 K and 70 K.

The silk fibroin film SF is predominantly diamagnetic, as clearly indicated by the negative slope of the linear curves of magnetic moment vs. H measured at T = 5 K and 70 K on the dried sample (Fig. S6). However, the different slope of the two curves is consistent with the presence of a paramagnetic signal at T = 5 K, which decreases with increasing temperature.

Heat maps of the gene expression overview

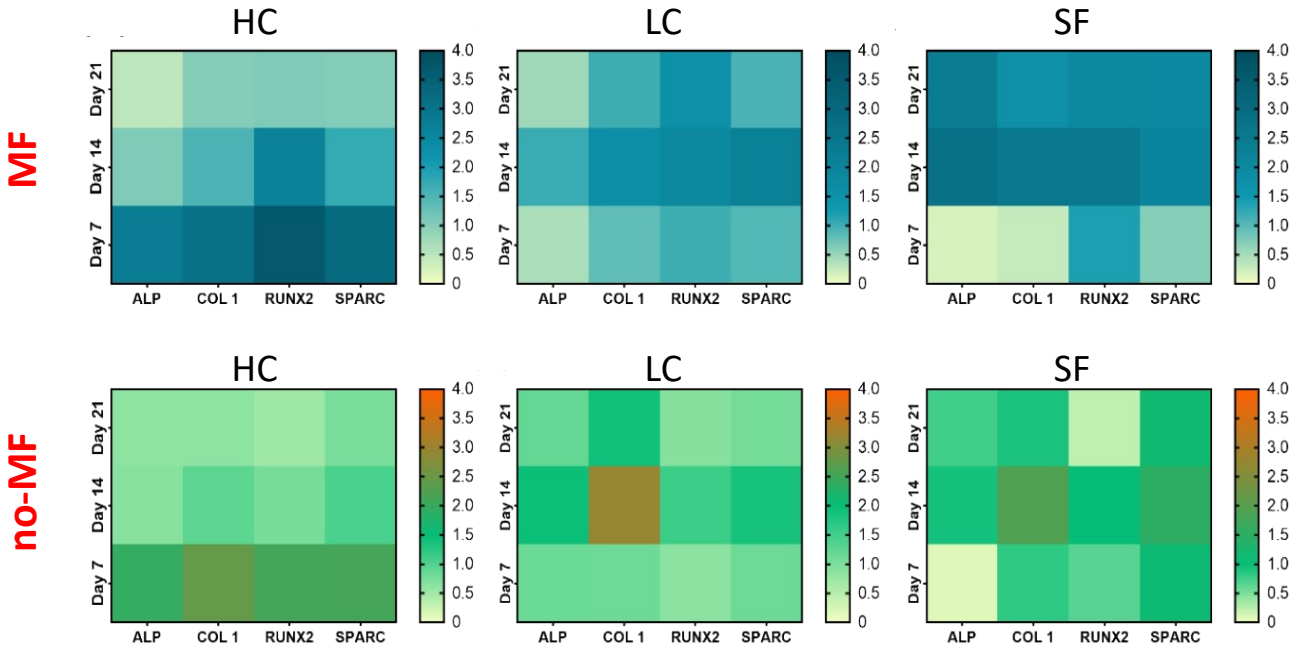

FIG. S7. Heat maps of gene expression levels of osteogenic differentiation markers of hMSCs cultured on HC, LC and SF films, under uniform magnetic field (MF, upper row) and without magnetic field (no-MF, lower row).

Table S1. Selected primers for gene expression

Gene	Primer	Catalog no.
ALP	ALPL, human	qHsaCID0010031
Collagen I	COL1A1, human	qHsaCED0043248
RUNX2	RUNX2, human	qHsaCED0044067
Osteonectin	SPARC, human	qHsaCID0010332
GAPDH	GAPDH, human	qHsaCED0038674

Numerical calculations for film LC

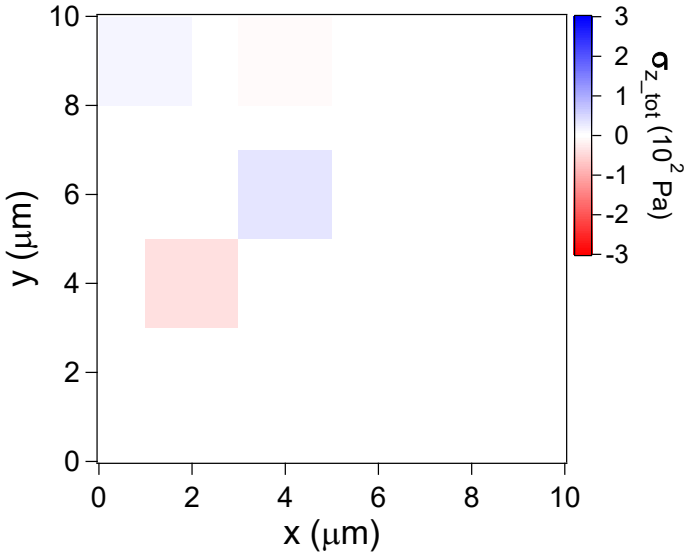

Fig. S8. Two-dimensional map related to the spatial distribution of σ_z for the assembly of simulated NP aggregates modeling the sample LC (Fig. 9b of the main article). The map is conceptually similar to that reported in Fig. 9f for sample HC. However, two main differences need to be highlighted. The first is that the color bar refers to a narrow range of values, i.e. $(-3 \div +3)\times 10^2$ Pa. The second difference is that the σ_z vectors with modulus smaller than σ_{silk_min} = 80 Pa are included, although they are not effective for triggering the magneto-mechanical stimulation of cells (otherwise, the figure would be completely white).

Mechanical tensile tests on film SF

The tensile tested samples are prepared by fixing strips obtained from the SF film on a paper frame provided with a square window of 1 cm side. The samples are fixed to the paper frame with a double-sided tape and by using super-glue. We used a MIDI 10 Machine. For this setup, we use a load cell of 10 N and test speed of 0.1 mm/s. The engineering stress is obtained by dividing the force by the cross-sectional area; the engineering strain is obtained by dividing the total displacement by the gauge length. The Young's modulus is found by fitting linearly the stress–strain curve and then calculating the slope.

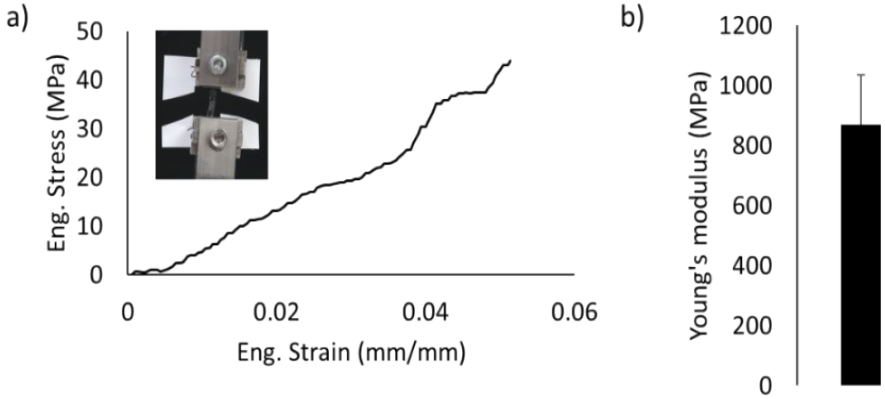

Fig. S9. a) Representative stress strain curve of SF; b) Young's modulus of SF as obtained from the tensile tests.

Calculation of the NP aggregates effective for cell stimulation assuming the Young's modulus value measured using the tensile method.

In the section 'Numerical Calculations' of the main article, the fraction of magnetic aggregates effective in the cell stimulation mechanism is calculated assuming that the Young's modulus of the dried silk fibroin matrix is ~ 8 GPa, as estimated by nanoindentation. One may observe that some literature articles report significantly lower values of the Young's modulus of silk, measured using the tensile method. We ourselves have verified that the Young's modulus derived from stress-strain measurements on macroscopic strips of the dried SF film is (0.9 ± 0.3) GPa (Fig. S9b), i.e. about an order of magnitude smaller than that estimated by nanoindentation. Most likely, this effect is correlated with the process of preparation of the sample's strip for the tensile test, which may induce the formation of defects and thus lead to an underestimation of the mechanical properties [Ref. 10]. However, if one considers that the Young's modulus of the SF film is this lower value, i.e. E_{silk} = 0.9 GPa, it follows that σ_{silk_max} = 900 Pa and, assuming a 100 times reduction of E_{silk} after wetting the film, σ_{silk_min} = 9 Pa. The purple dashed lines in Fig. S10 mark these values of σ_{silk_max} and σ_{silk_min}. The fraction of aggregates giving rise to $\sigma_z > \sigma_{silk\_max}$ is ~ 11% in the HC case and less than 1% in the LC one. As for the condition $\sigma_z > \sigma_{silk\_min}$, in the HC case, ~ 95% of the magnetic aggregates contribute effectively to cell stimulation, whereas the fraction of effective aggregates in the LC case is ~ 36 %. In fact, whatever the value of σ_{silk} is, between the two extremes σ_{silk_min} and σ_{silk_max}, Fig. S10 clearly shows that the effective fraction of aggregates is always larger in HC than in LC.

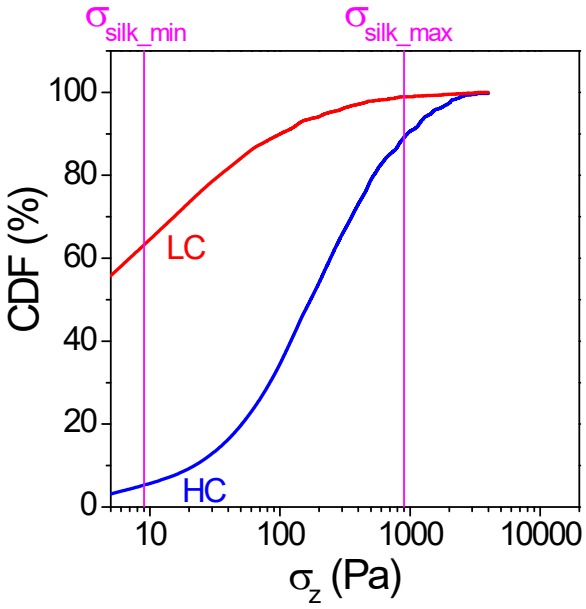

Fig. S10. Cumulative distribution function (CDF) of σ_z for the HC and LC cases.

Calculation of the stress produced on the silk fibroin matrix by an external magnetic field gradient.

With reference to the model drawn in Fig. 9a-b, a magnetic field gradient (grad**H**) applied along the z-axis generates a drag force, directed along the gradient, with modulus $F_{drag} = m \cdot |\text{grad}\mathbf{H}|$ on each NP aggregate, being m the modulus of the magnetic moment of the aggregate itself. Since the magnetic field gradient produced by placing a permanent magnet in the proximity of a cell-seeded substrate is typically of the order of 10 T/m [Refs. 3, 81], we set $|\text{grad}\mathbf{H}|$ = 50 T/m. Assuming that

the moment m of each aggregate is the same as in the simulation reported in the main article, the stress produced on the silk fibroin matrix by the smallest and largest aggregates (i.e. with radius = 50 nm and 500 nm) is 0.6 Pa and 6 Pa, respectively. Therefore, based on Fig. 9e and Fig. S10, the stress resulting from the dragging of the aggregates by the magnetic field gradient - considered as the only source of stress, i.e. neglecting that originating from the dipolar interactions between the aggregates, discussed in the main article - is too small to produce a deformation of the matrix that can be sensed by the cells.

Maps representing the dipolar magnetic field produced by the NP aggregates

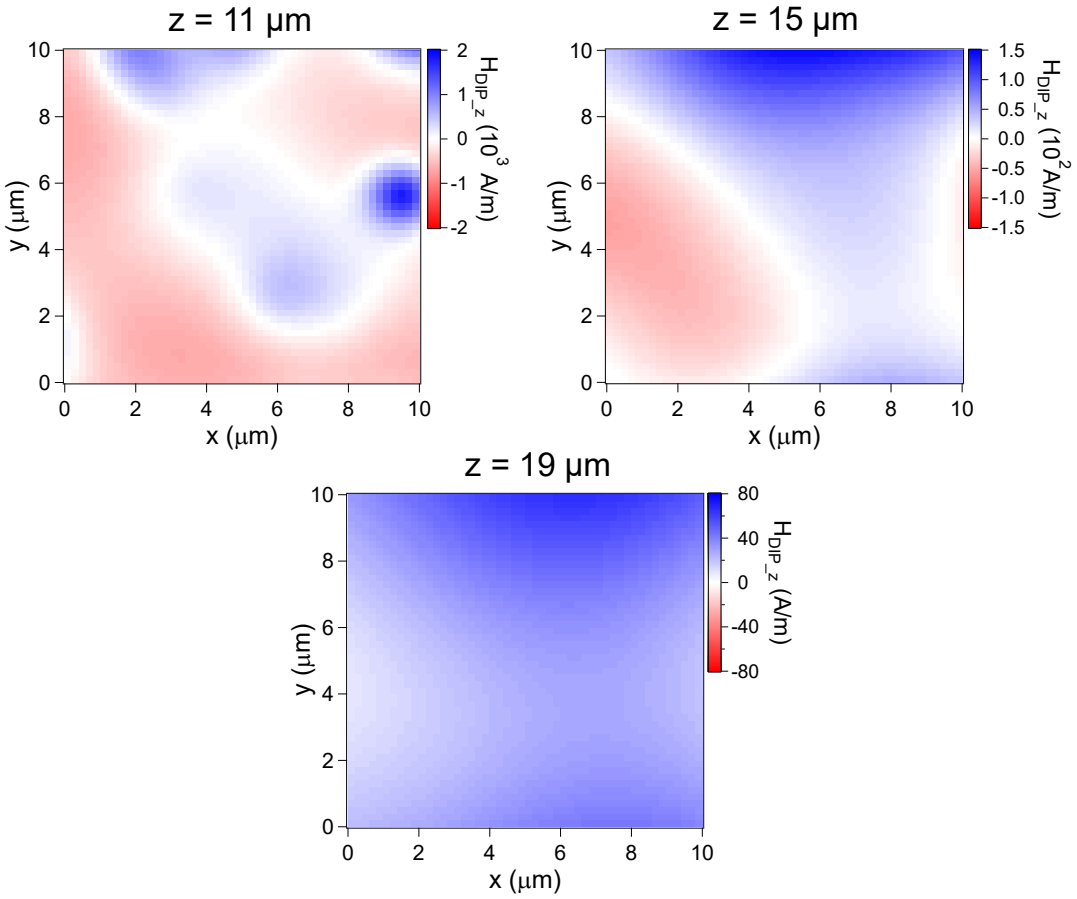

Fig. S11

The x-y maps in Fig. S11 provide information about the strength and sign of the z-component of the dipolar magnetic field (H_{DIP_z}) produced by the set of magnetic NPs shown in Fig. 9a (HC film). In particular, three maps are reported, computed at z = 11 μm, 15 μm, 19 μm. Hence, the maps correspond to three x-y planes in the region of space above the portion of film HC visualized in Fig. 9a, which, in our description, is occupied by the cell adhering to the film. As reported in the main text, the average value of H_{DIP_z} in the cubic volume of side 10 μm occupied by the cell is ~ 32 A/m, a value four orders of magnitude smaller than the magnetic field applied for the biological tests (~128 kA/m) and comparable to the Earth's magnetic field.

IRM and DCD curves

IRM is measured on an initially demagnetized sample, which is progressively magnetized by increasing the applied magnetic field H from 0 Oe up to 1.6×10^3 kA/m. The DCD measurement procedure is similar except that initially the sample is negatively saturated. The measured remanence values are plotted as a function of the previously applied magnetic field. The IRM and DCD curves are normalized to the final and initial value, respectively (Fig. S12).

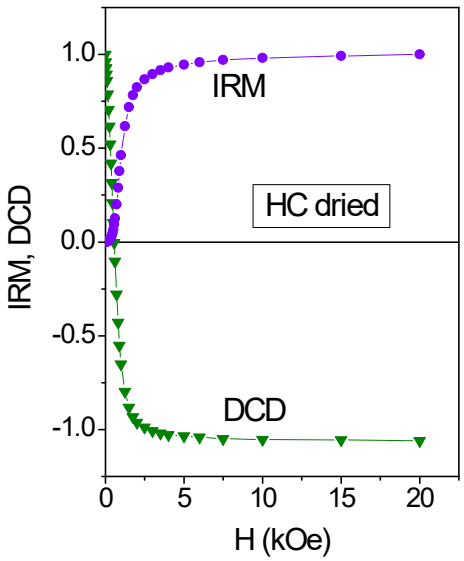

Fig. S12. Representative IRM and DCD curves measured by SQUID on the dried HC film at T = 5 K.

Magnet holder for setting up the external magnetic field for the *in vitro* biological tests

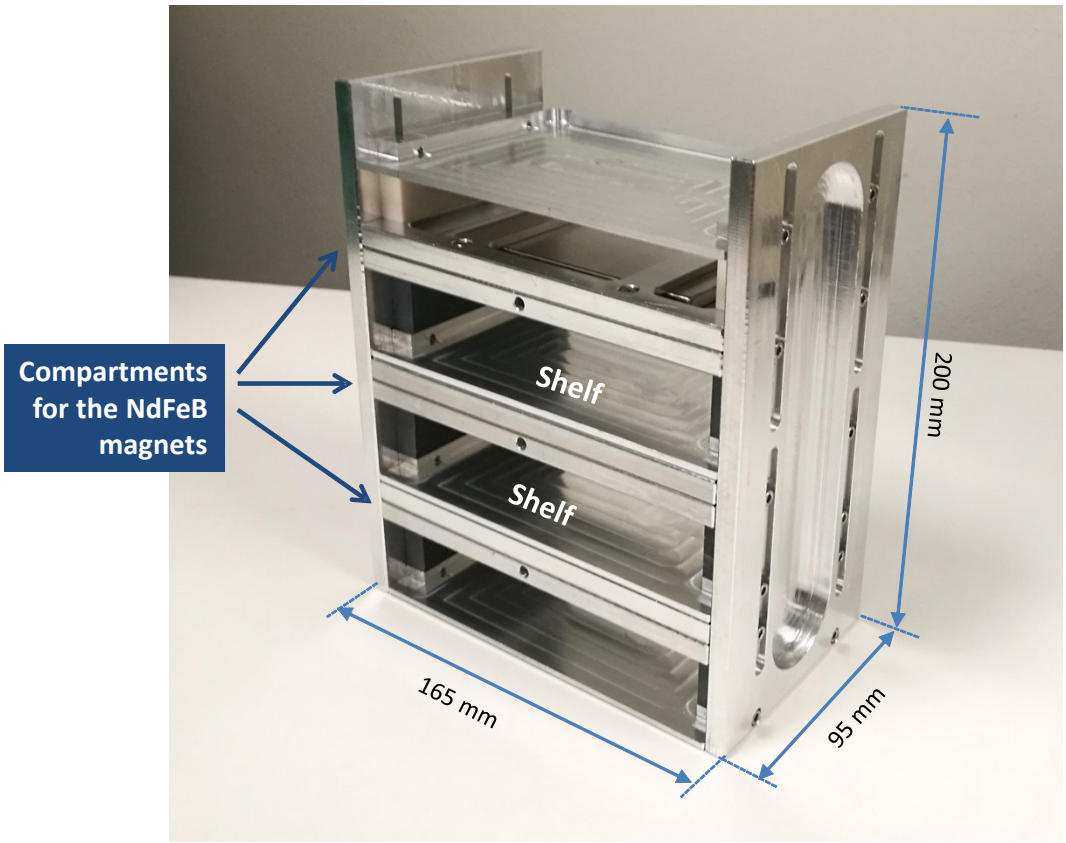

Fig. S13

Stem cells are cultured under a static uniform magnetic field using the custom-made holder for permanent magnets shown in Fig. S13. It is made of aluminum and has dimensions (95×165×200) mm^3. NdFeB magnets with dimensions (100 × 50 × 10) mm^3 are inserted in special compartments, in parallel configuration.

Two shelves are available to accommodate a cell culture plate, which is subjected to the uniform magnetic field produced by the pair of NdFeB magnets placed above and below it.

We use 48-wells culture plates. In order to be sure that the cells cultured in the wells are subjected to a magnetic field of similar intensity, the wells colored in red in the scheme here below are not used. At the positions of the remaining wells (colored in blue in the scheme) the magnetic field can be considered uniform and, for both shelves, the average value is H = (128 ± 8) kA/m.